CHEMISTRY OF MATERIALS
Article

Chem. Mater. **2010,** *22,* 2297–2308 2297
DOI:10.1021/cm903176d

Subnanometric Pd Particles Stabilized Inside Highly Cross-Linked Polymeric Supports

Elena Groppo,* Wei Liu, Olena Zavorotynska, Giovanni Agostini, Giuseppe Spoto, Silvia Bordiga, Carlo Lamberti, and Adriano Zecchina

Department of Inorganic, Physical and Materials Chemistry, NIS Centre of Excellence, and INSTM Unità di Torino, University of Torino, via Quarello 11, I-10135, Torino, Italy

Received October 15, 2009. Revised Manuscript Received January 15, 2010

Extremely small Pd nanoparticles have been successfully obtained from reduction of $Pd(OAc)_2$ precursor inside two highly cross-linked polymers, namely a poly(ethylstyrene) and a poly(4-vinylpyridine). The structural, optical, and vibrational properties of the Pd/polymer composites have been fully characterized by several techniques (FT-IR, UV−vis, and XAS spectroscopies, coupled with TEM microscopy) during all the synthetic steps. It is demonstrated that the nature of the polymeric matrix has a strong influence on the formation of the Pd nanoparticles and affect their final properties, in terms of particle size, electronic properties, and type and fraction of accessible surface sites. In particular, the presence of nitrogen-based ligands is at the base of the formation of extremely small, subnanometric Pd clusters in P4VP, as demonstrated by the observation of a specific interaction between Pd nanoparticles and the nitrogen of the pyridine ligands.

1. Introduction

Metal clusters and colloidal metal particles are attracting an increasing interest because of their unique properties and broad applicability in many fields, among which are microelectronics, chemical sensing, catalysis, to name only a few examples.[1−8] Physical and chemical properties of metal nanoparticles (NPs) depend on several factors, such as the particle size and size dispersity, the structure, the surface and the shape of the particle, and the organization of the particles on the support. In turn, all of these factors depend on the successful control of the synthetic process, thus explaining the big amount of work that has been devoted in the recent years to investigate the role played by the metal precursor, the reducing agent, the stabilizer, the synthesis conditions, etc., in controlling the particle size distribution and the structure of metal NPs.

Among all the investigated factors, the role of stabilizers is particularly important. Indeed, the formation of metal NPs necessarily requires stabilization to prevent aggregation, which would annul most of their desirable advantages compared with bulk materials of identical composition. Recently, numerous methods have been developed for the controlled synthesis of various metal nanoparticles in presence of different stabilizers, such as surfactants,[9] dendrimers,[10−13] functionalized polymers,[14−16] amphiphilic polymers,[17−21] and others. A standard strategy involves the use of weakly coordinated cationic precursor of the metal, which is then gently reduced. However, despite the enormous amount of literature on the topic, only a few studies have addressed the problem of how the ligand/stabilizer interacts with the metal NP, thus affecting its stabilization. Two main types of interactions can be identified: (i) Chaudret's group has demonstrated that when classical stabilizers are used, such as

*Corresponding author. Fax: +39 011 6707855. E-mail: elena.groppo@unito.it.

(1) *Metal Nanoparticles: Synthesis, Characterization and Applications*; Feldheim, D. L., Foss, C. A., Eds.; Marcel Dekker: New York, 2002.
(2) *Nanoparticles: From Theory to Application*; Schmid, G., Ed.; Wiley-VCH: Weinheim, Germany, 2004.
(3) Schmid, G. *Chem. Rev.* **1992**, *92*, 1709.
(4) Lewis, L. N. *Chem. Rev.* **1993**, *93*, 2693.
(5) Andres, R. P.; Bielefeld, J. D.; Henderson, J. I.; Janes, D. B.; Kolagunta, V. R.; Kubiak, C. P.; Mahoney, W. J.; Osifchin, R. G. *Science* **1996**, *273*, 1690.
(6) Schmid, G.; Baumle, M.; Geerkens, M.; Helm, I.; Osemann, C.; Sawitowski, T. *Chem. Soc. Rev.* **1999**, *28*, 179.
(7) Rao, C. N. R.; Kulkarni, G. U.; Thomas, P. J.; Edwards, P. P. *Chem. Soc. Rev.* **2000**, *29*, 27.
(8) Shipway, A. N.; Katz, E.; Willner, I. *ChemPhysChem* **2000**, *1*, 18.
(9) LizMarzan, L. M.; LadoTourino, I. *Langmuir* **1996**, *12*, 3585.
(10) Yeung, L. K.; Lee, C. T.; Johnston, K. P.; Crooks, R. M. *Chem. Commun.* **2001**, 2290.
(11) Yeung, L. K.; Crooks, R. M. *Nano Lett.* **2001**, *1*, 14.
(12) Fahmi, A.; D'Aleo, A.; Williams, R. M.; De Cola, L.; Gindy, N.; Vogtle, F. *Langmuir* **2007**, *23*, 7831.
(13) Worden, J. G.; Dai, Q.; Huo, Q. *Chem. Commun.* **2006**, 1536.
(14) Toshima, N.; Harada, M.; Yonezawa, T.; Kushihashi, K.; Asakura, K. *J. Phys. Chem.* **1991**, *95*, 7448.
(15) Bradley, J. S.; Hill, E. W.; Behal, S.; Klein, C.; Chaudret, B.; Duteil, A. *Chem. Mater.* **1992**, *4*, 1234.
(16) Pathak, S.; Greci, M. T.; Kwong, R. C.; Mercado, K.; Prakash, G. K. S.; Olah, G. A.; Thompson, M. E. *Chem. Mater.* **2000**, *12*, 1985.
(17) Seregina, M. V.; Bronstein, L. M.; Platonova, O. A.; Chernyshov, D. M.; Valetsky, P. M.; Hartmann, J.; Wenz, E.; Antonietti, M. *Chem. Mater.* **1997**, *9*, 923.
(18) Klingelhofer, S.; Heitz, W.; Greiner, A.; Oestreich, S.; Forster, S.; Antonietti, M. *J. Am. Chem. Soc.* **1997**, *119*, 10116.
(19) Bronstein, L.; Kramer, E.; Berton, B.; Burger, C.; Forster, S.; Antonietti, M. *Chem. Mater.* **1999**, *11*, 1402.
(20) Schlotterbeck, U.; Aymonier, C.; Thomann, R.; Hofmeister, H.; Tromp, M.; Richtering, W.; Mecking, S. *Adv. Funct. Mater.* **2004**, *14*, 999.
(21) Zheng, P. W.; Jiang, X. W.; Zhang, X.; Zhang, W. Q.; Shi, L. Q. *Langmuir* **2006**, *22*, 9393.

Published on Web 02/24/2010

carboxylic acids, thiols, or amines, a σ-type coordination between the heterodonor atom of the stabilizer and the metallic surface is established.[22] (ii) Recently, Kobayashi's group has reported a new method for preparing polymer-supported metal NPs, based on microencapsulation and cross-linking.[23−28] The authors assumed that in these systems metal NPs were immobilized on the polymeric support by means of electronic interaction between the π-electrons of the benzene rings of the polystyrene-based polymers and the vacant orbitals of metal atoms. To design specific ligands and/or stabilizers, it is of prime importance to understand how they are coordinated at the NP surface.[29]

The use of polymers as supports for metal NPs has drawn particular attention, because of the unique physical-chemical properties and attractive catalytic performance of the resultant supported metals.[24,30−36] In particular, heterogeneous and heterogenized polymer supported Pd-based catalysts have shown remarkable performance in coupling and hydrogenation reactions.[37−40] The advantage of these catalysts with respect to their homogeneous counterparts are the greater stability and the easier recoverability. Since the properties of the Pd NPs strongly depend on the type of interaction with the polymeric support, it would be of great interest a detailed investigation on how the nature of the polymer influences the formation of the Pd NPs and their final properties.

This work is focused on the synthesis and complete characterization of Pd NPs encapsulated inside two highly DVB cross-linked polymeric supports, namely a poly(ethylstyrene) and a poly(4-vinylpyridine). In two recent works, it has been demonstrated that a systematic and careful multitechnical approach is needed to fully characterize supported nanoparticles.[41,42] Starting from this experience, here we apply EXAFS, UV−vis, and FT-IR spectroscopies, coupled with TEM microscopy, to investigate the structural, optical, and vibrational properties of the two Pd/polymer systems in all the synthetic steps, starting from the hosted $Pd(OAc)_2$ precursors up to Pd NPs. We demonstrate that the nature of the polymeric supports has a strong influence on the properties of the hosted Pd NPs, in terms of reducibility of the Pd precursor, particle size distribution, optical properties, and type and fraction of accessible surface sites. Finally, it is worth noticing that the two supports present a permanent porosity, a condition that should allow, in principle, the investigation of catalytic reactions in the gas phase.

2. Experimental Section

2.1. Sample Preparation. Two polymeric matrices, 25% cross-linked with divinylbenzene, were adopted as supports in this work: a poly(divinylbenzene-co-4-vinylpyridine) (hereafter P4VP) and a poly(4-ethylstyrene-co-divinylbenzene) (hereafter PS), both of them commercialized by Aldrich. Their surface area and porous structure have been evaluated by N_2 adsorption at 77 K, carried on a Micromeritics ASAP 2020 sorption analyzer resulting into a BET surface area of 52 $m^2\ g^{-1}$ and 1000 $m^2\ g^{-1}$ for P4VP and PS, respectively. The DFT (density functional theory) analysis allowed also the determination of the distribution of the pores on the basis of the slit model, evidencing the presence of two different families of pores in both polymers: one in the 12−21 Å range (micropores) and a second broader distribution of pores having width > 20 Å (mesopores).

Pd/polymers composites were obtained by impregnating the polymeric supports with a solution of $Pd(OAc)_2$ in acetonitrile, resulting into a Pd concentration of ∼2 and 5 wt % in the P4VP and PS case, respectively. The as-prepared samples were successively subjected to the following treatments: (i) outgassing procedure at 120 °C for 1 h in dynamic vacuum, and (ii) reduction in a H_2 atmosphere at 120 °C. The reduction process consists of two subsequent H_2 dosages (equilibrium pressure P_{H2} = 120 Torr, 1 Torr = 133.3 Pa, contact time = 15 min). After the last H_2 removal at the reduction temperature down to $P_{H2} < 1 \times 10^{-4}$ Torr, the samples were cooled to room temperature in a dynamic vacuum. These procedures were carried out in the same cells used for the characterization. At each step, several in situ spectroscopic techniques were employed in order to investigate the structural, vibrational, and optical properties of the confined Pd phase.

2.2. Techniques. *XAS.* X-ray absorption experiments, at the Pd K-edge (24350 eV), were performed at the BM26A beamline of the ESRF facility (Grenoble, F).[43a] The white beam was monochromatized using a Si(111) double crystal; harmonic rejection has been performed using Pt-coated silicon mirrors. The following experimental geometry was adopted: (1) I_0 (10% efficiency); (2) sample; (3) I_1 (40% efficiency); (4) reference Pd foil; (5) I_2 (80% efficiency). This setup allows a direct energy/angle calibration for each spectrum avoiding any problem related to little energy shifts due to small thermal instability of the monochromator crystals.[43b] EXAFS part of the spectra was

(22) Pan, C.; Pelzer, K.; Philippot, K.; Chaudret, B.; Dassenoy, F.; Lecante, P.; Casanove, M. J. *J. Am. Chem. Soc.* **2001**, *123*, 7584.
(23) Okamoto, K.; Akiyama, R.; Yoshida, H.; Yoshida, T.; Kobayashi, S. *J. Am. Chem. Soc.* **2005**, *127*, 2125.
(24) Akiyama, R.; Kobayashi, S. *Chem. Rev.* **2009**, *109*, 594.
(25) Akiyama, R.; Kobayashi, S. *Angew. Chem., Int. Ed.* **2001**, *40*, 3469.
(26) Akiyama, R.; Kobayashi, S. *Angew. Chem., Int. Ed.* **2002**, *41*, 2602.
(27) Kobayashi, S.; Akiyama, R. *Chem. Commun.* **2003**, 449.
(28) Akiyama, R.; Kobayashi, S. *J. Am. Chem. Soc.* **2003**, *125*, 3412.
(29) Favier, I.; Massou, S.; Teuma, E.; Philippot, K.; Chaudret, B.; Gomez, M. *Chem. Commun.* **2008**, 3296.
(30) Lu, J.; Toy, P. H. *Chem. Rev.* **2009**, *109*, 815.
(31) Erathodiyil, N.; Ooi, S.; Seayad, A. M.; Han, Y.; Lee, S. S.; Ying, J. Y. *Chem.—Eur. J.* **2008**, *14*, 3118.
(32) Xing, R.; Liu, Y. M.; Wu, H. H.; Li, X. H.; He, M. Y.; Wu, P. *Chem. Commun.* **2008**, 6297.
(33) Kanaoka, S.; Yagi, N.; Fukuyama, Y.; Aoshima, S.; Tsunoyama, H.; Tsukuda, T.; Sakurai, H. *J. Am. Chem. Soc.* **2007**, *129*, 12060.
(34) Miyamura, H.; Matsubara, R.; Miyazaki, Y.; Kobayashi, S. *Angew. Chem., Int. Ed.* **2007**, *46*, 4151.
(35) Weck, M.; Jones, C. W. *Inorg. Chem.* **2007**, *46*, 1865.
(36) Hong, Y. Y.; Sen, A. *Chem. Mater.* **2007**, *19*, 961.
(37) Bronstein, L. M.; Chernyshov, D. M.; Volkov, I. O.; Ezernitskaya, M. G.; Valetsky, P. M.; Matveeva, V. G.; Sulman, E. M. *J. Catal.* **2000**, *196*, 302.
(38) Caporusso, A. M.; Innocenti, P.; Aronica, L. A.; Vitulli, G.; Gallina, R.; Biffis, A.; Zecca, M.; Corain, B. *J. Catal.* **2005**, *234*, 1.
(39) Phan, N. T. S.; Van Der Sluys, M.; Jones, C. W. *Adv. Synth. Catal.* **2006**, *348*, 609.
(40) Evangelisti, C.; Panziera, N.; Pertici, P.; Vitulli, G.; Salvadori, P.; Battocchio, C.; Polzonetti, G. *J. Catal.* **2009**, *262*, 287.
(41) Agostini, G.; Pellegrini, R.; Leofanti, G.; Bertinetti, L.; Bertarione, S.; Groppo, E.; Zecchina, A.; Lamberti, C. *J. Phys. Chem. C* **2009**, *113*, 10485.
(42) Berthoud, R.; Délichère, P.; Gajan, D.; Lukens, W.; Pelzer, K.; Basset, J.-M.; Candy, J.-P.; Copéret, C. *J. Catal.* **2008**, *260*, 387.
(43) (a) Nikitenko, S.; Beale, A. M.; van der Eerden, A. M. J.; Jacques, S. D. M.; Leynaud, O.; O'Brien, M. G.; Detollenaere, D.; Kaptein, R.; Weckhuysen, B. M.; Bras, W. *J. Synchrotron Radiat.* **2008**, *15*, 632. (b) Lamberti, C.; Bordiga, S.; Bonino, F.; Prestipino, C.; Berlier, G.; Capello, L.; D'Acapito, F.; Xamena, F. X. L. I.; Zecchina, A. *Phys. Chem. Chem. Phys.* **2003**, *5*, 4502.

collected with a variable sampling step in energy, resulting in $\Delta k = 0.05$ Å^{-1}, up to 20 Å^{-1}, with an integration time that linearly increases with k from 4 to 25 s/point to account for the low signal-to-noise ratio at high k values. Samples, in the form of self-supported pellets of optimized thickness, have been located inside an ad hoc conceived cell that allows in situ evacuation, gas dosage and warming and cooling. The extraction of the $\chi(k)$ function was performed using Athena code.[44] For each sample, 2 consecutive EXAFS spectra have been collected and corresponding $\chi(k)$ functions have been averaged before data analysis. EXAFS data analysis was performed using the Arthemis software.[44] Phase and amplitudes were calculated by FEFF6 code,[45] and successfully checked with Pd metal foil. For each sample, the averaged $k^3\chi(k)$ functions were Fourier transformed in the $\Delta k = 2.00-16.00$ Å^{-1} interval.

UV−Vis DR. UV−vis spectra have been collected in diffuse reflectance mode (DR), on samples in the powdered form, inside a homemade cell equipped with a cuvette in optical quartz, allowing us to perform thermal treatments and measurements in controlled atmosphere. The spectra have been collected on a Cary 5000 instrument, equipped with a reflectance sphere.

FT-IR. For the in situ FT-IR measurements the samples have been measured in transmission mode in the form of self-supporting pellets, inside an IR quartz cell where thermal treatments and measurement in controlled atmosphere can be performed. After the reduction step, all the outgassed samples were contacted in situ with CO (P_{CO} = 50 Torr). The FT-IR spectra were recorded at room temperature at 2 cm^{-1} resolution, using a Bruker IFS66 instrument, equipped with a MCT detector. P_{CO} was then gradually reduced in steps from 50 to 1×10^{-4} Torr. After each step, the FT-IR spectrum of remaining adsorbed CO species was acquired. The final spectrum corresponds to CO species irreversibly adsorbed at room temperature.

HRTEM. High-resolution transmission electron micrographs (HRTEM) were obtained with a JEOL 3010-UHR instrument operating at 300 kV, equipped with a 2k × 2k pixels Gatan US1000 CCD camera. Samples were deposited on a copper grid covered with a lacey carbon film. Particle size distributions were obtained counting at least 200 particles. To present the data uniformly, a class width of 2 Å was chosen for all the particle size distributions. As the sample exhibited very small Pd particles, proper contrast/sampling conditions were set by: (a) counting only Pd particles found on regions of the support thin enough to appreciate the smallest contrast differences and (b) acquiring images at a magnification of 400k× (0.026 nm per pixel). However, it must be considered that particles with diameter below 10 Å might escape the detection by this technique.

3. Results and Discussion

3.1. Fresh Pd(OAc)$_2$/Polymer Samples. The fresh Pd/polymer samples were investigated by means of several complementary techniques before any kind of treatments. The XANES spectra of Pd(OAc)$_2$ inside PS and P4VP (red and orange curves in Figure 1a, respectively) are very similar to the spectrum of bulk Pd(OAc)$_2$ (brown curve in Figure 1a), in both the edge and the white-line (i.e., first resonance after the edge) regions. This suggests that the

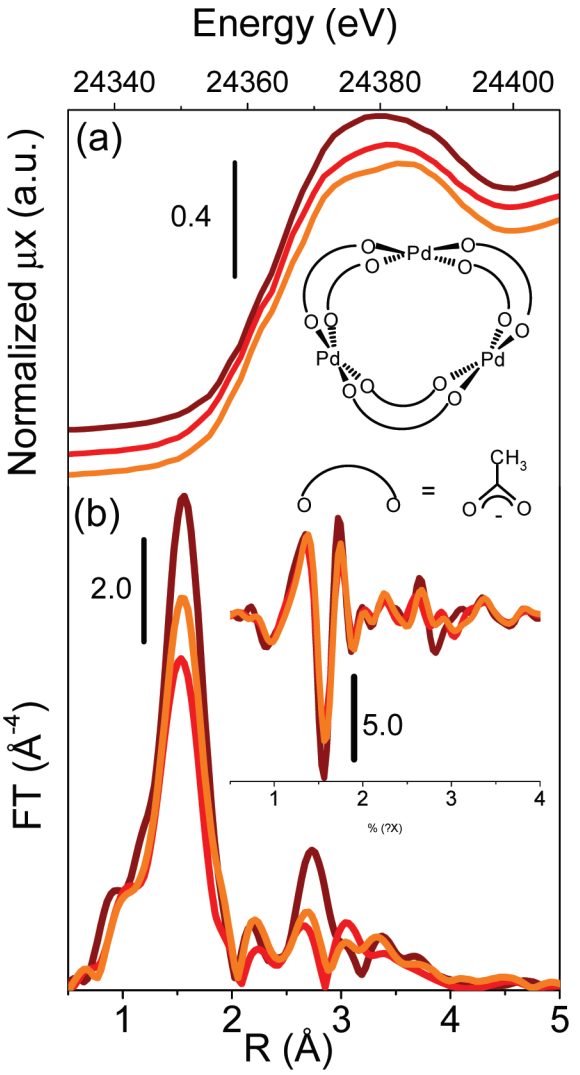

Figure 1. (a) XANES (spectra vertically translated for clarity) and (b) |FT| of the k^3-weighted EXAFS spectra of Pd(OAc)$_2$ in PS (red curves) and P4VP (orange curves) polymeric matrices, compared to bulk Pd(OAc)$_2$ reference samples (brown curves). Inset in (b) reports the corresponding Imm(FT), whereas inset in a shows (a) schematic representation of the trimeric structure of bulk Pd(OAc)$_2$.

oxidation state of Pd is Pd^{2+} (no reduction occurs on the fresh samples) and that the local environment around the absorbing atom is very similar to that of the Pd(OAc)$_2$ precursor.

Bulk Pd(OAc)$_2$ has a trimeric structure and contains a bridging acetate (see inset in Figure 1a). It is interesting to observe that the triangular (Pd^{II})$_3$ moiety is a rarity, since most polynuclear Pd^{II} complexes contain linear (Pd^{II})$_n$ structures. More in details, in the crystalline form of Pd(OAc)$_2$ (as determined by XRD)[46] the Pd ions occupy the corners of a (nearly) equilateral triangle. Each pair of Pd^{II} ions is bridged by two acetate groups in which the two equivalent O atoms are directed toward each Pd ion, with Pd−O distances in the 1.973−2.014 Å range and Pd−Pd nonbonded distance in the 3.105−3.203 Å region. The EXAFS datum for bulk Pd(OAc)$_2$ is in perfect agreement with the crystallographic structure. The |FT|

(44) Ravel, B.; Newville, M. *J. Synchrotron Radiat.* **2005**, *12*, 537.
(45) Ankudinov, A. L.; Ravel, B.; Rehr, J. J.; Conradson, S. D. *Phys. Rev. B* **1998**, *58*, 7565.
(46) Skapski, A. C.; Smart, M. L. *Chem. Commun.* **1970**, 658.

Table 1. Summary of the Parameters Optimized by Fitting the EXAFS Data of $Pd(OAc)_2$ Bulk (reference) and Fresh Pd/PS and Pd/P4VP Samples[a]

	$Pd(OAc)_2$ bulk	Pd/PS fresh	Pd/P4VP fresh
ΔE_0 (eV)	-3 ± 1	-2 ± 1	-2 ± 1
N_O	4	3.4 ± 0.4	3.5 ± 0.4
S_0^2	0.9 ± 0.1	0.9	0.9
R_{Pd-O} (Å)	2.004 ± 0.006	2.007 ± 0.008	2.009 ± 0.008
σ^2_{Pd-O} (Å^{-2})	0.0025 ± 0.0006	0.0041 ± 0.0008	0.0028 ± 0.0008
R_{factor}	0.022	0.023	0.028

[a] The fits were performed on the first coordination sphere (ΔR = 1.0−2.0 Å) over FT of the k^3-weighted $\chi(k)$ functions performed in the Δk = 2.0−16.0 Å^{-1} interval, resulting into a number of independent parameters of $2\Delta R\Delta k/\pi$ = 8.9. Non optimized parameters are recognizable by the absence of the corresponding error bar.

of the k^3-weighted EXAFS spectrum for bulk $Pd(OAc)_2$ (brown curve in Figure 1b) is characterized by a main component centered at 1.56 Å (distance not corrected in phase) because of the four oxygen neighbors and by a less intense but well-defined feature centered at 2.74 Å (distance not corrected in phase), which is mainly due to the contribution of two Pd neighbors (2.4 ± 1.0) at an average distance of 3.11 ± 0.02 Å. Additional contributions from C atoms of the acetate groups are present in this region and have to be considered in the model used to fit the data. However, to compare with the $Pd(OAc)_2$/polymer samples, the fit was performed on the first shell only (see first column in Table 1 and fit reported in Figure S1 of the Supporting Information), resulting in S_0^2 = 0.9 ± 0.1 and R_{Pd-O} = 2.004 ± 0.006 Å, with a Debye−Waller factor of 0.0025 ± 0.0006 Å^{-2}, typical of well-ordered materials.

The |FT| of the k^3-weighted EXAFS spectra for $Pd(OAc)_2$ dispersed inside the polymeric matrices (red and orange curves in Figure 1b) present a first coordination sphere very similar to that of bulk $Pd(OAc)_2$, only slightly lower in intensity, whereas the Pd−Pd component due to the longer Pd−Pd nonbonding distance is completely absent (in both modulus and imaginary parts, see inset in Figure 1b). A summary of the optimized parameters is reported in Table 1, whereas the related fits are reported in Figure S1 of the Supporting Information. A slightly lower N_O coordination number (rescaled on the S_0^2 obtained for the reference $Pd(OAc)_2$) and slightly higher σ^2_{Pd-O} values have been obtained. The decrease of the coordination number, the increase of the σ^2_{Pd-O}, and the disappearance of the Pd−Pd contribution can be explained in terms of a heterogeneous distortion of the trimeric structure of $Pd(OAc)_2$, or of its complete rupture into dimers and/or monomers. On the basis of the EXAFS data only, discrimination between these two possibilities cannot be done.

It is well-known that the trimeric $Pd(OAc)_2$ is soluble in glacial acetic acid[47] or less polar solvents such as benzene[48,49] and acetonitrile. In these solvents, the Pd-

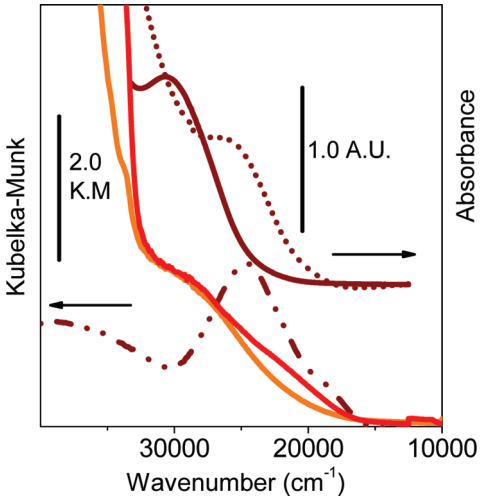

Figure 2. DR UV−vis spectra of $Pd(OAc)_2$ in PS and P4VP (red and orange curves, respectively) polymeric supports, compared to reference samples (brown curves). Bulk $Pd(OAc)_2$ diluted in SiO_2 has been measured in DR mode (dotted-dashed brown line), whereas $Pd(OAc)_2$ in pyridine (full brown line) and acetonitrile (dotted brown line) have been measured in transmission mode (spectra vertically translated for clarity).

$(OAc)_2$ complex retains its trimeric composition and gives rise to a broad absorption in the UV−vis spectrum, with a band maximum around 25000 cm^{-1} (400 nm), as reported in Figure 2 (dotted brown curve). The high intensity and energy of this band suggests that it involves ligand-to-metal charge transfer from the acetate ligands to the Pd ions. It is worth noticing that a similar UV−vis spectrum is observed in the case of bulk $Pd(OAc)_2$ (dashed-dotted brown curve in Figure 2), which is characterized in this case by a tail at lower frequencies, typical for solid-state materials. However, upon addition of alkali metal acetates to solutions of $Pd_3(OAc)_6$, the trimeric structure breaks down, with the consequent change of the absorption spectrum, that shifts toward higher frequencies (up to 27 600 cm^{-1}, 362 nm).[47,50] A similar behavior of the optical spectra is observed when $Pd(OAc)_2$ is dissolved in pyridine (full brown curve in Figure 2), showing a maximum centered around 30 000 cm^{-1} (330 nm). This suggests that one or two acetate ligands are substituted by pyridine units, with the consequent decomposition of the trimeric structure. A more complex situation is observed in the case of $Pd(OAc)_2$ dispersed inside PS and P4VP. In both cases a very broad component centered around 28000 cm^{-1} (360 nm) is observed, with a pronounced tail extending down to 20 000 cm^{-1} (500 nm); note that the strong absorption at frequencies higher than 32 000 cm^{-1} is due to the $\pi-\pi^*$ transitions characterizing the polymeric matrix. The absence of a well-defined component and the large range of frequency over which the spectra are extended are in agreement with the heterogeneity of species suggested by EXAFS data, and can be interpreted both in terms of distortion or rupture of the $Pd(OAc)_2$ trimeric structure.

Finally, the FT-IR spectra of the fresh $Pd(OAc)_2$/polymer samples have been compared to those of the

(47) Kragten, D. D.; van Santen, R. A.; Crawford, M. K.; Provine, W. D.; Lerou, J. J. *Inorg. Chem.* **1999**, *38*, 331.
(48) Zabinsky, S. I.; Rehr, J. J.; Ankudinov, A.; Albers, R. C.; Eller, M. J. *Phys. Rev. B* **1995**, *52*, 2995.
(49) Stephenson, T. A.; Morehouse, S. M.; Powell, A. R.; Heffer, J. P.; Wilkinson, G. *J. Chem. Soc.* **1965**, 3632.
(50) Pandey, R. N.; Henry, P. M. *Can. J. Chem.* **1974**, *52*, 1241.

corresponding polymeric matrixes (spectra not shown). In both cases only the vibrational manifestation related with the acetate groups emerge from the spectrum of the polymeric background. No changes are observed in the vibrational modes of the polymers, suggesting that no specific interactions occur between the hosted $Pd(OAc)_2$ precursor and the supports. This is not straightforward, at least in the case of P4VP. Several examples are reported in literature regarding the formation of complexes between P4VP and metal complexes or small molecules, where a shift of the vibrational modes related with the pyridine units is observed.[51−58] In the present case, the trimeric structure of $Pd(OAc)_2$ maybe responsible for the absence of a specific interaction with pyridine.

3.2. In situ Reduction of $Pd(OAc)_2$/Polymer Samples. *3.2.1. XANES Spectroscopy*. Once that the structural, optical and vibrational properties of fresh $Pd(OAc)_2$/polymer samples have been determined, their reducibility as a function of temperature and atmosphere was investigated.

XANES spectroscopy is a valuable technique to evaluate the degree of $Pd^{2+} \rightarrow Pd^0$ reduction, because the position of the edge and the white line features are associated with the oxidation state of the absorbing species and their local environment. The XANES spectra of both samples at each step of reduction are reported in Figure 3, and compared to those of bulk $Pd(OAc)_2$ (dotted orange) and Pd foil (black), used as reference for Pd^{2+} and Pd^0 species, respectively. In the case of Pd/PS sample (Figure 3a), a gradual evolution in both edge and white line regions is observed upon treatment at 120 °C in vacuum and in H_2 atmosphere (from orange, to brown and gray curves). In particular, the edge gradually shifts toward lower energy down to the Pd foil value, accompanied by a decrease of the white line intensity and the appearance of three isosbestic points at 24 370, 24 390, and 24 405 eV, that clearly demonstrate that the Pd^{2+} species are transformed into Pd^0. By contrast to the Pd/PS system, in the case of Pd/P4VP sample no changes in the XANES spectrum are observed upon outgassing at 120 °C (orange and brown curves in Figure 3b); only when reduced in H_2 at the same temperature (gray curve in Figure 3b) a shift of the edge position toward the Pd foil and a decrease in the white line intensity are observed.

A quantitative evaluation of the fraction of Pd^{2+} and Pd^0 species in the two investigated samples is possible by fitting the XANES data with a linear combination of the spectra of the two reference compounds.[59,60] This procedure requires the definition of the energy interval in which the fit is performed. In this regard, it is important to observe that the first EXAFS oscillation of Pd metal appears immediately after the edge (negative and positive peaks at 24382 and 24397 eV, respectively). These strong features are due to the well-arranged local fcc structure, where 12 Pd atoms are coordinated at the same distance from the central Pd atom. Therefore, the intensity of these features contains intrinsically information on the Pd particle size. When the size of Pd metal particles is small, there is a large fraction of low coordinated atoms, causing low amplitude of the EXAFS oscillation. Therefore, only a small energy range close to the edge (from −20 eV to +25 eV) is available for the quantitative evaluation of the fraction of reduced species.[61] The results of the fit (performed without imposing any constraints) are resumed in the inset of Figure 3a. It is clear that the thermal decomposition of $Pd(OAc)_2$ is greater when it is dispersed

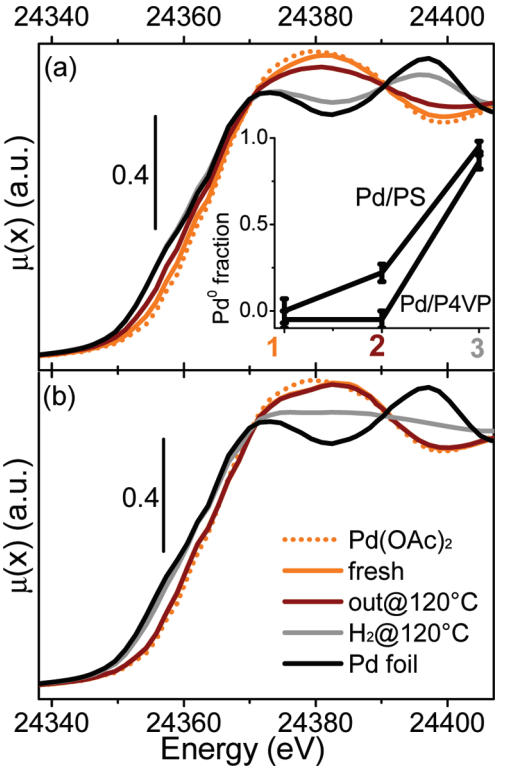

Figure 3. XANES spectra of (a) Pd/PS and (b) Pd/P4VP samples at different treatment steps: fresh (orange), outgassed at 120 °C (brown), and H_2 reduced at 120 °C (gray), compared to $Pd(OAc)_2$ (dotted orange) and Pd foil (black), used as references for Pd^{2+} and Pd^0 species. Inset in a reports the Pd^0 fraction at each step as evaluated by a linear combination of the spectra of the two references.

(51) Groppo, E.; Uddin, M. J.; Zavorotynska, O.; Damin, A.; Vitillo, J. G.; Spoto, G.; Zecchina, A. *J. Phys. Chem. C* **2008**, *112*, 19493.
(52) Groppo, E.; Uddin, M. J.; Bordiga, S.; Zecchina, A.; Lamberti, C. *Angew. Chem., Int. Ed.* **2008**, *47*, 9269.
(53) Pardey, A. J.; Rojas, A. D.; Yanez, J. E.; Betancourt, P.; Scott, C.; Chinea, C.; Urbina, C.; Moronta, D.; Longo, C. *Polyhedron* **2005**, *24*, 511.
(54) Wu, K. H.; Wang, Y. R.; Hwu, W. H. *Polym. Degrad. Stab.* **2003**, *79*, 195.
(55) Belfiore, L. A.; McCurdie, M. P.; Das, P. K. *Polymer* **2001**, *42*, 9995.
(56) McCurdie, M. P.; Belfiore, L. A. *Polymer* **1999**, *40*, 2889.
(57) Belfiore, L. A.; Graham, H.; Ueda, E. *Macromolecules* **1992**, *25*, 2935.
(58) Lyons, A. M.; Vasile, M. J.; Pearce, E. M.; Waszczak, J. V. *Macromolecules* **1988**, *21*, 3125.
(59) Lamberti, C.; Prestipino, C.; Bonino, F.; Capello, L.; Bordiga, S.; Spoto, G.; Zecchina, A.; Moreno, S. D.; Cremaschi, B.; Garilli, M.; Marsella, A.; Carmello, D.; Vidotto, S.; Leofanti, G. *Angew. Chem., Int. Ed.* **2002**, *41*, 2341.
(60) Le Toquin, R.; Paulus, W.; Cousson, A.; Prestipino, C.; Lamberti, C. *J. Am. Chem. Soc.* **2006**, *128*, 13161.
(61) Note that the assumption that the edge position scales linearly as a function of the oxidation state could be questionable for small nanoparticles, because their electronic properties could be affected by ligand binding and support interaction. However, in the present case, the complete reduction of Pd^{2+} upon treatment in H_2 is demonstrated by independent FTIR measurements (vide infra).

inside PS matrix, but in both cases an almost complete reduction is achieved (within the experimental error) upon treatment in H_2 at 120 °C. Nevertheless, the intensity of the first EXAFS oscillation is highly different in the two cases, suggesting that the average size of the obtained particles is much smaller in the Pd/P4VP case. Note that the Pd-$(OAc)_2$/PS is not definitely stable in air, but undergoes a progressive reduction with time. This does not occur in the case of Pd$(OAc)_2$/P4VP, testifying that the two systems are also characterized by a different stability.

3.2.2. UV−Vis Spectroscopy. The reduction of Pd-$(OAc)_2$/polymer samples was followed also by means of in situ UV−vis DR spectroscopy. Typically, electronic spectra of metal nanoclusters (such as Cu, Ag, and Au) show strong absorption bands due to the excitation of the surface plasmon resonance (i.e., coherent oscillation of the conduction band electrons induced by the interacting electromagnetic fields). These bands can be correlated to physical properties using theoretical approaches, such as Mie theory, and in principle the maximum of the plasmon resonance can be correlated to the nanoparticle dimension.[62] In particular, the larger the particle's dimension, the lower the frequency of the absorption maximum (or the higher the λ). The problem is that many transition metals, including Pd, do not show distinct plasmon peaks in the visible region. Moreover, it is well-known that when the diameter of a metal nanoparticle is reduced, the electronic energy levels become quantized because of the confinement of the electrons into smaller dimensions of the particles and, as a result, metal-to-nonmetal transition occurs at a certain critical size. For these reason, very few works report the optical spectra of Pd nanoparticles. An in situ UV−vis investigation on Pd nanoparticles formation in solution has been presented by Rothenberg's group,[63] showing the growth of a broad absorption extended in all the visible region. Authors demonstrate that the traditional band assignment approach, which works well for well-defined homogeneous complexes, does not provide an accurate description when nanoclusters are concerned. This is exactly what we observe in the Pd/polymers case.

Reduction in H_2 at 120 °C causes an evident change in the color of the samples that from bright orange (orange curve in Figure 4) turn dark gray and light gray-brown in the case of Pd/PS and Pd/P4VP samples, respectively. The correspondent UV−vis spectra are reported in Figure 4 (gray curves). For both samples, the spectra are characterized by a broad absorption band that extends down to 15 000 cm^{-1} in the Pd/P4VP case, and to 8000 cm^{-1} in the Pd/PS one. Whatever is the origin of the broad absorption bands shown by the two Pd/polymer composites, two important observations must be done: (1) the absorption bands cover a different frequency region, the Pd/PS system absorbing at lower frequencies with respect to Pd/P4VP; (2) in both Pd/PS and Pd/P4VP cases, the broad absorption is affected by exposure to air (red curves in Figure 4), being almost completely destroyed in the Pd/P4VP case, and only slightly diminished in the Pd/PS one. This last behavior definitely validates the assignment of the broad absorption appearing in the UV−vis spectra upon H_2 reduction to formation of Pd nanoparticles. The different position and the different reactivity toward exposure to air should be related to a different particle dimension, as will be discussed in the following sections.

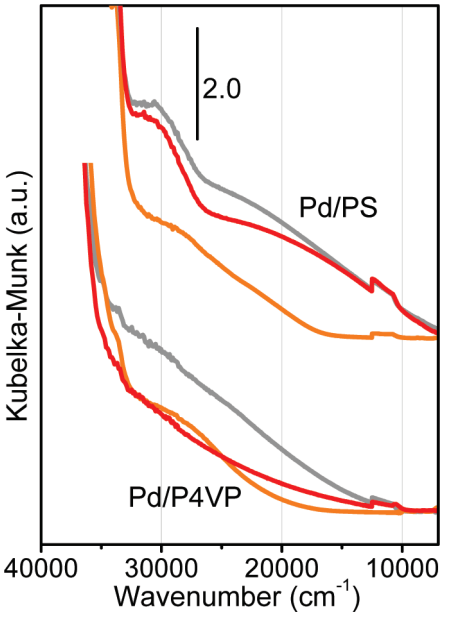

Figure 4. UV−vis DRS spectra of Pd/PS (upper part) and Pd/P4VP (bottom part) at different subsequent steps of activation: fresh (orange), H_2 reduced at 120 °C (gray) and after exposure to air (red).

3.3. Properties of the Pd Nanoparticles and Their Interaction with the Polymeric Support. *3.3.1. Direct Observation of the Pd Nanoparticles: TEM Results*. XANES and UV−vis spectroscopies suggest that the nature of the polymeric matrix influences the reducibility of the hosted Pd-$(OAc)_2$ precursor as well as the dimension of the resulting Pd nanoparticles. To have a direct insight into the size distribution of Pd particles, an accurate TEM investigation was conducted. Representative HRTEM images of the two samples are reported in Figure 5. Few particles are visible in the Pd/PS case (a), with a different size in the 10−60 Å range, whereas much more particles are observed in the case of Pd/P4VP (b), with a higher homogeneous dispersion and smaller sizes. In both cases the particles present a spherical shape and there is no evidence of well-defined exposed surfaces. This will be confirmed by FT-IR spectroscopy of adsorbed CO (see section 3.3.2).

A systematic TEM analysis on a statistically significant number of particles allowed us to estimate the relative particle size distribution in the two cases (see insets in Figure 5). A quite asymmetric and broad distribution is observed for Pd/PS, with a relevant tail at higher diameter values, suggesting a heterogeneous situation and the occur-

(62) (a) Evanoff, D. D.; Chumanov, G. *J. Phys. Chem. B* **2004**, *108*, 13957. (b) Evanoff, D. D.; Chumanov, G. *ChemPhysChem* **2005**, *6*, 1221. (c) Agostini, G.; Usseglio, S.; Groppo, E.; Uddin, M. J.; Prestipino, C.; Bordiga, S.; Zecchina, A.; Solari, P. L.; Lamberti, C. *Chem. Mater*. **2009**, *21*, 1343.

(63) (a) Wang, J.; Boelens, H. F. M.; Thathagar, M. B.; Rothenberg, G. *ChemPhysChem* **2004**, *5*, 93. (b) Gaikwad, A. V.; Rothenberg, G. *Phys. Chem. Chem. Phys*. **2006**, *8*, 3669.

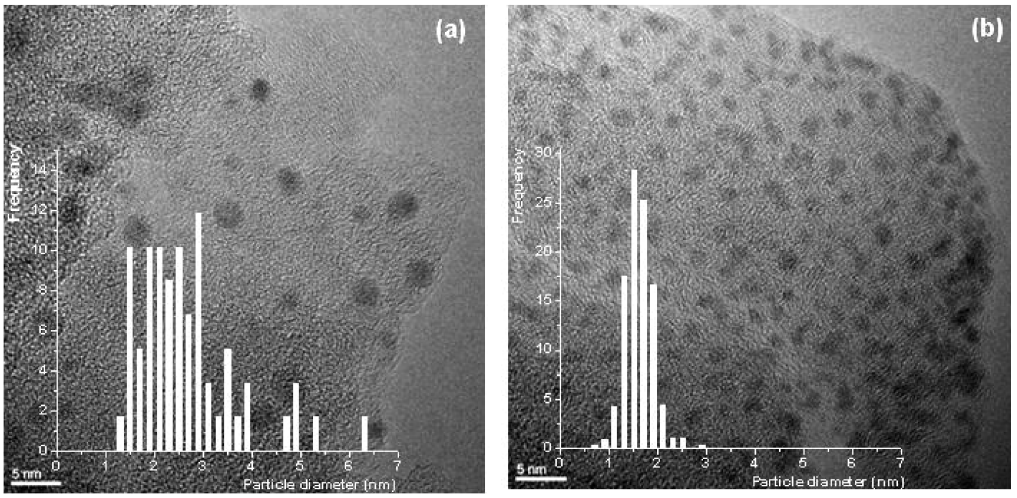

Figure 5. Representative TEM images of Pd nanoparticles formed inside (a) PS and (b) P4VP samples, and corresponding particle size distributions.

rence of some sintering. The estimated average particle size is 27 Å, with a standard deviation of 10 Å. The absence of particles with very small diameter is an intrinsic problem of the technique, which hardly detects particles with size smaller than 10 Å. A much more symmetric and narrow distribution is obtained for the Pd/P4VP sample, as the diameter of most of the particles lies in the 5−25 Å range, with an average particle size of 16 Å and a standard deviation of 3 Å. It is important to notice that no particles bigger than 30 Å are observed in this case and 50% of the counted particles are smaller than 15 Å.

3.3.2. Available Surface Sites: FT-IR Results. TEM images evidenced that the Pd nanoparticles obtained inside PS and P4VP polymers are characterized by a different particle size distribution and UV−vis spectroscopy suggested that they experience a different electronic environment. Both differences can be potentially probed also by means of FT-IR of adsorbed CO, which is a well-established technique to obtain information on the exposed faces of supported metal nanoparticles and on their defectivity.[41,64−75] Figure 6b,c report the FT-IR spectra of CO dosed at 300 K on the Pd/polymer samples H_2-reduced at 120 °C, upon decreasing CO coverage (θ). In our experimental conditions, θ_{max} (bold black curve) corresponds to T = 300 K and P_{CO} = 50 Torr, whereas θ_{min} (bold gray curve) is obtained by evacuation at 300 K down to 1×10^{-4} Torr. At a first look it is evident that in the Pd/P4VP case the spectra present an overall higher intensity (notice the different scale in parts b and c). This is the first immediate proof that Pd dispersion is much higher in Pd/P4VP than in Pd/PS, nicely confirming TEM results.

Coming in more detail, in the case of the Pd/PS sample (Figure 6b), the highest coverage spectrum (bold black curve) is characterized by two main components at 2072 and 1926 cm^{-1}, respectively, with an almost equal intensity (see Table 2). On the basis of the huge amount of literature on the topic,[64,68,70,76−90] these two components

(64) Tessier, D.; Rakai, A.; Bozonverduraz, F. *J. Chem. Soc., Faraday Trans.* **1992**, *88*, 741.
(65) Craciun, R.; Daniell, W.; Knozinger, H. *Appl. Catal., A* **2002**, *230*, 153.
(66) Pestryakov, A. N.; Lunin, V. V.; Fuentes, S.; Bogdanchikova, N.; Barrera, A. *Chem. Phys. Lett.* **2003**, *367*, 102.
(67) Skotak, M.; Karpinski, Z.; Juszczyk, W.; Pielaszek, J.; Kepinski, L.; Kazachkin, D. V.; Kovalchuk, V. I.; d'Itri, J. L. *J. Catal.* **2004**, *227*, 11.
(68) Bertarione, S.; Scarano, D.; Zecchina, A.; Johanek, V.; Hoffmann, J.; Schauermann, S.; Frank, M. M.; Libuda, J.; Rupprechter, G.; Freund, H. J. *J. Phys. Chem. B* **2004**, *108*, 3603.
(69) van der Eerden, A. M. J.; Visser, T.; Nijhuis, A.; Ikeda, Y.; Lepage, M.; Koningsberger, D. C.; Weckhuysen, B. M. *J. Am. Chem. Soc.* **2005**, *127*, 3272.
(70) Lear, T.; Marshall, R.; Gibson, E. K.; Schutt, T.; Klapotke, T. M.; Rupprechter, G.; Freund, H. J.; Winfield, J. M.; Lennon, D. *Phys. Chem. Chem. Phys.* **2005**, *7*, 565.
(71) Lear, T.; Marshall, R.; Lopez-Sanchez, J. A.; Jackson, S. D.; Klapotke, T. M.; Baumer, M.; Rupprechter, G.; Freund, H. J.; Lennon, D. *J. Chem. Phys.* **2005**, *123*, 174706.
(72) Lear, T.; Marshall, R.; Lopez-Sanchez, J. A.; Jackson, S. D.; Klapotke, T. M.; Baumer, M.; Rupprechter, G.; Freund, H. J.; Lennon, D. *J. Chem. Phys.* **2006**, *124*, 069901.
(73) Bertarione, S.; Prestipino, C.; Groppo, E.; Scarano, D.; Spoto, G.; Zecchina, A.; Pellegrini, R.; Leofanti, G.; Lamberti, C. *Phys. Chem. Chem. Phys.* **2006**, *8*, 3676.
(74) Groppo, E.; Bertarione, S.; Rotunno, F.; Agostini, G.; Scarano, D.; Pellegrini, R.; Leofanti, G.; Zecchina, A.; Lamberti, C. *J. Phys. Chem. C* **2007**, *111*, 7021.
(75) Bollmann, L.; Ratts, J. L.; Joshi, A. M.; Williams, W. D.; Pazmino, J.; Joshi, Y. V.; Miller, J. T.; Kropf, A. J.; Delgass, W. N.; Ribeiro, F. H. *J. Catal.* **2008**, *257*, 43.
(76) Xu, X. P.; Goodman, D. W. *J. Phys. Chem.* **1993**, *97*, 7711.
(77) Xu, X. P.; Chen, P. J.; Goodman, D. W. *J. Phys. Chem.* **1994**, *98*, 9242.
(78) Freund, H. J. *Angew. Chem., Int. Ed.* **1997**, *36*, 452.
(79) Wolter, K.; Seiferth, O.; Libuda, J.; Kuhlenbeck, H.; Baumer, M.; Freund, H. J. *Chem. Phys. Lett.* **1997**, *277*, 513.
(80) Wolter, K.; Seiferth, O.; Libuda, J.; Kuhlenbeck, H.; Baumer, M.; Freund, H. J. *Surf. Sci.* **1998**, *404*, 428.
(81) Wolter, K.; Seiferth, O.; Kuhlenbeck, H.; Bäumer, M.; Freund, H. J. *Surf. Sci.* **1998**, *399*, 190.
(82) Henry, C. R. *Surf. Sci. Rep.* **1998**, *31*, 235.
(83) Surnev, S.; Sock, M.; Ramsey, M. G.; Netzer, F. P.; Wiklund, M.; Borg, M.; Andersen, J. N. *Surf. Sci.* **2000**, *470*, 171.
(84) Freund, H. J.; Baumer, M.; Kuhlenbeck, H. *Adv. Catal.* **2000**, *45*, 333.
(85) Sheppard, N.; De La Cruz, C. *Catal. Today* **2001**, *70*, 3.
(86) Ozensoy, E.; Goodman, D. W. *Phys. Chem. Chem. Phys.* **2004**, *6*, 3765.
(87) Henrich, V. E.; Cox, P. A. *The Surface Science of Metal Oxides*; Cambridge University Press: Cambridge, U.K., 1994.
(88) Barteau, M. A. *Chem. Rev.* **1996**, *96*, 1413.
(89) Barteau, M. A.; Vohs, J. M. Oxide model systems. In *Handbook of Heterogeneous Catalysis*; Ertl, G., Knözinger, H., Weitkamp, J., Ed.; Wiley-VCH: Weinheim, Germany, 1997; Vol. *2*, p. 873.
(90) Xu, C.; Goodman, D. W. Ultrathin oxide films: model catalyst supports. In: *Handbook of Heterogeneous Catalysis*; Ertl, G.; Knözinger, H.; Weitkamp, J., Ed.; Wiley-VCH: Weinheim, Germany, 1997; Vol. *2*, p 826.

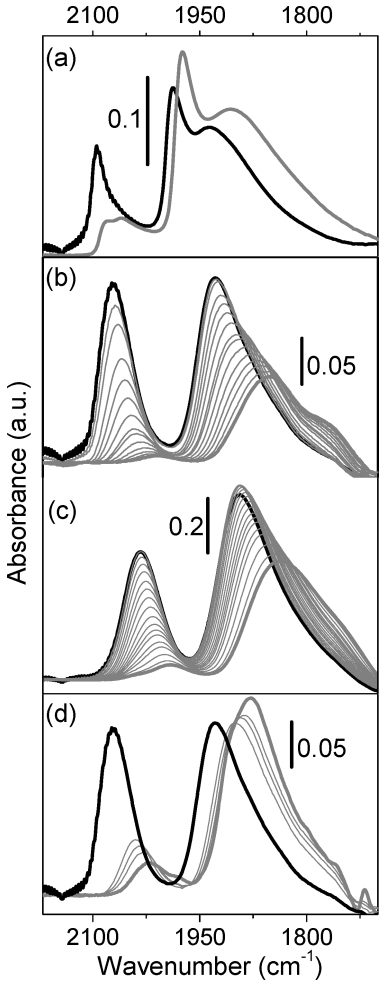

Figure 6. FT-IR spectra of CO dosed at room temperature on the (b) Pd/PS and (c) Pd/P4VP H_2-reduced at 120 °C. The sequences of spectra show the effect of decreasing P_{CO}, from 50 (bold black curve) to 1×10^{-4} Torr (bold gray curve). (a) For comparison, the θ_{max} (black) and θ_{min} (gray) spectra of CO adsorbed on a $Pd/SiO_2-Al_2O_3$ sample activated in the same conditions and characterized by an average particle size of 28 Å.[91] (d) Effect of dosing pyridine vapor pressure on a Pd/PS sample previously contacted with P_{CO} = 50 Torr. Black curve, same as in b. Bold gray curve, maximum coverage of pyridine; thin gray curves, effect of decreasing pyridine pressure by keeping constant P_{CO}.

are assigned to linear and bridged CO species, respectively. The usual assignment in terms of CO adsorbed on well-defined Pd faces is problematic for NPs because the prediction of a well-defined geometrical model is difficult in the case of nanoparticles smaller than 20 Å. As a term of comparison, we report the spectrum at θ_{max} obtained in the case of CO adsorbed on a $Pd/SiO_2-Al_2O_3$ sample activated in the same conditions (black spectrum in Figure 6a), characterized by a homogeneous particle size distribution centered around 28 Å, with a well-defined cuboctahedral shape.[91]

The following main differences are observed.

(1) For CO adsorbed on Pd/PS, the component due to linear carbonyls is broader and less defined, suggesting the presence of a greater variety of terminal carbonyls, as expected in the case of highly defective and/or amorphous nanoparticles.[15,68,73,92,93] Moreover, it is shifted at lower frequencies (appearing close to 2100 cm^{-1} in the same experimental conditions on well-defined cuboctahedral Pd particles, see black curve in Figure 6a). This is usually observed in the case of small nanoparticles, where the coupling of the CO oscillators is not completely effective.

(2) The component due to bridged carbonyls on (100) face (band at 1990 cm^{-1} in the case of well-defined cuboctahedral NPs) is totally absent, confirming that a cuboctahedral model is not valid in this case, as already suggested by TEM images.

(3) The linear and bridged components present an almost equal intensity. This is a further proof in favor of the presence of very small and/or amorphous nanoparticles. Indeed, investigation on CO adsorbed on colloidal metal nanoparticles revealed that there is a correlation between the particle size and the relative proportion of linear and bridged adsorbed carbonyls.[15,92] Small and probably amorphous metal particles exhibit prevalently linear (terminal) CO species, whereas an increase in the particle size results in a greater number of bridged carbonyls.

(4) Finally, the carbonyl species are easily reversible. Both bands decrease in intensity and gradually downward shift upon lowering θ (from thin gray spectra to bold gray): the band due to linear carbonyls shifts from 2072 to 2008 cm^{-1} and almost disappears upon prolonged outgassing, whereas the component due to bridged carbonyls moves from 1926 to 1852 cm^{-1} (see Table 2). This behavior is particular relevant, especially if compared with the $Pd/SiO_2-Al_2O_3$ sample, where the majority of both linear and bridged CO species is irreversible also after prolonged outgassing (gray curve in Figure 6a).[41,91] The easier reversibility of adsorbed CO reveals that the polymeric support plays an "active" role and competes with CO in interacting with Pd NPs surface. A similar behavior was previously reported in the case of molecular Pd carbonyl clusters hosted in zeolites,[94] for which a chemical interaction of zeolite walls with the Pd clusters was fully established.

The CO adsorption on Pd/P4VP sample shows a similar behavior, with three important differences. (1) As already anticipated at the beginning of this section, the spectra present an overall higher intensity, as expected for better dispersed NPs. (2) All the components are

Table 2. ν(CO) (cm^{-1}) of the Different Type of Carbonyls (linear/bridged) Formed on Pd/PS and P4VP[a]

	Pd/PS	Pd/P4VP
linear	2072/2008	2033/1991
bridged	1926/1852	1893/1835

[a] Black and grey values refer to the highest and lowest coverages explored in the work, respectively, corresponding to the bold black and bold grey spectra reported in Figure 6.

(91) Pellegrini, R.; Leofanti, G.; Agostini, G.; Bertinetti, L.; Bertarione, S.; Groppo, E.; Zecchina, A.; Lamberti, C. *J. Catal.* **2009**, *267*, 40.
(92) Bradley, J. S.; Millar, J. M.; Hill, E. W.; Behal, S. *J. Catal.* **1991**, *129*, 530.
(93) Sheu, L. L.; Karpinski, Z.; Sachtler, W.-M. H. *J. Phys. Chem.* **1989**, *93*, 4890.
(94) Sheu, L.-L.; Knozinger, H.; Sachtler, W.-M. H. *J. Am. Chem. Soc.* **1989**, *111*(8), 8125.

downward shifted with respect to what occurs on the Pd/PS sample. In particular, the component due to linear carbonyls appears at 2033 cm^{-1} (at θ_{max}) and shifts downward to 1991 cm^{-1} upon lowering θ, whereas the component assigned to the bridged species shifts from 1893 to 1835 cm^{-1} upon lowering P_{CO} (see Table 2). The downward shift ($\Delta\nu$ around -35 cm^{-1} at θ_{max}) of both linear and bridged carbonyls bands with respect to Pd/PS sample should be explained by the different electronic environment which Pd nanoparticles experience in the two polymeric matrices. Indeed, the nitrogen atom of the pyridil ligands in P4VP should act as electron donor, thus increasing the π-back-donation from Pd particles to the adsorbed CO molecules. (3) Finally, the downward shift of the carbonyl bands upon decreasing θ is lower for Pd/P4VP than for Pd/PS (-42 vs -64 cm^{-1}); this is again perfectly in agreement with the smaller size of the NPs, the shift being associated with the coupling of the CO oscillators on the surface.

To fully demonstrate the role of Py ligands in affecting the electronic properties of Pd NPs, we performed an ad hoc experiment (Figure 6d). CO was dosed on Pd/PS sample (black spectrum in Figure 6d), followed by exposure to the vapor pressure of pyridine (bold gray spectrum in Figure 6c). The effect on the FT-IR spectrum is spectacular: both linear and bridged CO bands are immediately shifted to the lower frequency; in addition, the linear component is strongly affected in intensity. The new position of the two components is very close to that observed for CO adsorbed on Pd/P4VP sample (Figure 6c). Next, pyridine was condensed in a liquid nitrogen trap, which allowed to reduce pyridine pressure on the sample and simultaneously keep the pressure of CO almost constant. The IR bands of the adsorbed CO then moved back toward the original ones (thin gray curves in Figure 6c).

From the whole set of FT-IR experiments (Figure 6), it can be definitely concluded that pyridil ligands of P4VP support closely surround Pd NPs and affect their electronic properties, with important consequences on the properties of the adsorbed CO molecules. Pyridil moieties are stronger ligands with respect to CO molecules, and therefore they cannot be displaced by incoming CO. A qualitative representation of this situation is depicted in Figure 7 for a Pd NP with a diameter around 10 Å. It is expected that the presence of pyridil ligands close to Pd surface would play a relevant role when Pd/P4VP sample is employed in catalysis.

3.3.3. EXAFS Spectroscopy. Last but not least, EXAFS spectroscopy can provide complementary information with respect to the previous techniques, being sensitive to bulk as well as surface Pd species. The EXAFS spectra of Pd/polymers at each activation step are reported in Figure 8 and compared to those of the reference compounds. From a qualitative inspection of the spectra, it is possible to get information on the reducibility of the $Pd(OAc)_2$ species hosted in the polymeric matrices, similar to those already discussed in the case of the XANES data (see Figure 3). Moreover, a quantitative

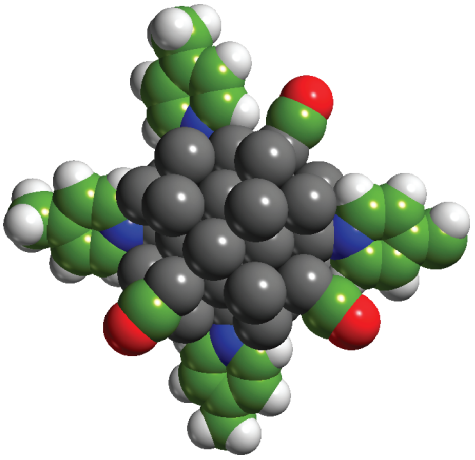

Figure 7. Qualitative representation of a Pd nanoparticle surrounded by pyridil ligands and by CO molecules. All the atoms are represented as CPK spheres. Color code: Pd, gray; C, green; O, red; N, blue; and H, white.

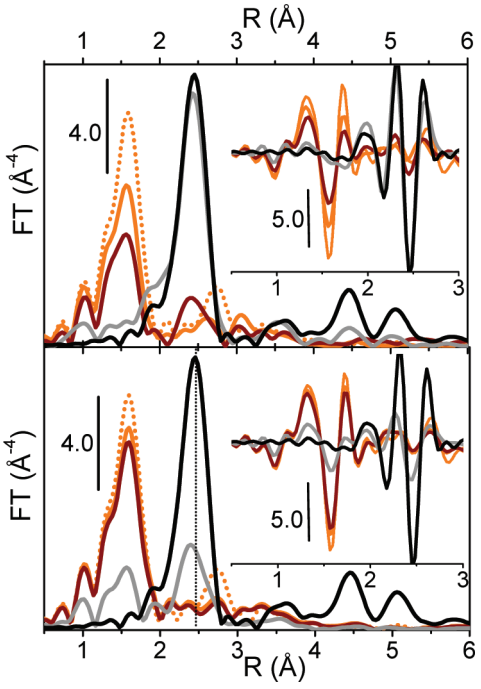

Figure 8. Moduli (main part) and imaginary parts (insets) of the FT of the k^3-weighted $\chi(k)$ functions for (a) Pd/PS and (b) Pd/P4VP samples at different treatment steps: fresh (orange), outgassed at 120 °C (brown), and H_2 reduced at 120 °C (gray), compared to $Pd(OAc)_2$ (dotted orange) and Pd foil (black), used as references for Pd^{2+} and Pd^0 species. Note that the spectrum of Pd foil has been divided for 3.3. Vertical line in b shows the shift in the Pd−Pd contribution between the Pd/P4VP sample and the reference Pd foil.

data analysis could provide information on the local structure around Pd atoms.

In the case of the Pd/PS sample, a decrease in the Pd−O contribution centered around 1.56 Å (not corrected in phase) is observed upon outgassing at 120 °C (brown curve in Figure 8a), accompanied by the appearance of a new component at 2.41 Å, because of Pd−Pd contribution of metal nanoparticles. This behavior confirms that a fraction of $Pd(OAc)_2$ is reduced to Pd metal in these conditions, in agreement with the XANES analysis.

Table 3. Summary of the Parameters Optimized by Fitting the EXAFS Data of Pd/PS and Pd/P4VP Samples Reduced in H_2 at 120°C, Compared to Pd Foil[a]

	Pd bulk	Pd/PS H_2@120 °C	Pd/P4VP H_2@120 °C	
ΔR (Å)	1.6−3.0	1.6−3.0	1.6−3.0	1.0−3.0
ΔE_0 (eV)	−5.1 ± 0.5	−7 ± 1	−8 ± 1	−8 ± 1
N_{Pd}	12	6.8 ± 0.5	3.9 ± 0.8	3.9 ± 0.6
S_0^2	0.92 ± 0.04	0.92	0.92	0.92
R_{Pd-Pd} (Å)	2.743 ± 0.004	2.736 ± 0.006	2.71 ± 0.01	2.713 ± 0.007
σ^2_{Pd-Pd} (Å^{-2})	0.0060 ± 0.0005	0.0089 ± 0.0007	0.012 ± 0.012	0.012 ± 0.001
$S_0^2 N_N$				1.3 ± 0.3
R_{Pd-N} (Å)				2.011 ± 0.009
σ^2_{Pd-N} (Å^{-2})				0.004 ± 0.001
R_{factor}	0.002	0.007	0.085	0.032

[a] The fits were performed over FT of the k^3-weighted $\chi(k)$ functions performed in the 2.0−16.0 Å^{-1} interval, in the ΔR range specified for each column. Non optimized parameters are recognizable by the absence of the corresponding error bar.

When treated in H_2 at 120 °C (gray curve in Figure 8c), the Pd−O component is completely destroyed and the Pd−Pd peak reaches its maximum value, which is however 3.3 times less intense than that obtained in the case of Pd foil, as expected for small Pd particles. It is worth noticing that the higher shell multiple scattering contributions centered around 4.5 and 5.0 Å (distances not corrected in phase) are visible in this case, even if characterized by a very weak intensity.

The average Pd coordination number obtained by a first shell analysis of the EXAFS datum for Pd/PS reduced in H_2 at 120 °C is 6.8 ± 0.5, vs 12 of the bulk, with a Debye−Waller factor $\sigma^2_{Pd-Pd} = 0.0089 \pm 0.0004$ Å^{-2} (see Table 3 and Figure S2 in the Supporting Information). In principle, indirect information on the average particle size of the Pd metal particles can be obtained from EXAFS data analysis, provided that an appropriate geometrical model is chosen. Given the difficulty associated with developing a deterministic model that can uniquely define both the shape and size of a cluster, EXAFS studies of supported NPs typically assume, either implicitly or explicitly, that the particles adopt quasi-hemispherical shapes, and the evolution of the average first shell Pd−Pd coordination number (N_{Pd}) versus Pd particle diameter have been computed for hemispherical clusters (cuboctahedral, spherical, etc.).[23,41,95−97] In the present case, if a cuboctahedral model is assumed, an average coordination number close to 7 should correspond to particle diameter around 11.5 Å.[41] An analogous value is obtained by assuming a spherical model.[23] However, in the case of particles with diameters smaller than 30 Å, prediction of the most stable structure is difficult[98,99] and the average Pd−Pd coordination number is a strong and nonlinear function of the particle diameter. For this reason, as carefully demonstrated by Frenkel et al.,[95,97] a first shell analysis cannot unambiguously provide for an understanding of the coordination numbers and Debye−Waller factor values in the first shell bond lengths, and the first shell coordination numbers cannot be interpreted in a strict quantitative structural sense. On this consideration, we will come back later, when comparison will be done with TEM data (see section 3.3.4).

Coming to the Pd/P4VP sample, EXAFS spectroscopy confirms that no reduction occurs upon outgassing at 120 °C (compare brown and orange curves in Figure 8b), whereas big changes are observed in the EXAFS spectrum after H_2 reduction at 120 °C (gray spectrum in Figure 8b). Also in this case, a new peak appears in the Pd−Pd region, but slightly shifted toward lower distances with respect to that of Pd foil (more evident in the imaginary part, see inset in Figure 8b) and much lower in intensity. A preliminary fit on this peak (see last but one column in Table 3: (ΔR = 1.6−3.0 Å) gives an extremely small average N_{Pd} value (3.9 ± 0.8), with an average $R_{Pd-Pd} = 2.71 \pm 0.01$ Å, i.e., 0.03 Å smaller than that of bulk Pd. No evidence of the higher shell contributions is visible in this case. Beside the peak due to the Pd−Pd contribution, an important contribution at lower distances is also present, centered around 1.56 Å. At the first look, this peak could be interpreted as a Pd−O contribution resulting from a significant fraction of unreduced $Pd(OAc)_2$. This interpretation, which could also explain the very low intensity of the Pd−Pd contribution, must however be discarded on the basis of (i) the XANES analysis previously discussed (see section 3.2.1), demonstrating that almost all Pd^{2+} species are reduced to Pd^0 within the accuracy of the technique (10%) and (ii) FT-IR of adsorbed CO, showing no bands due to Pd^{2+} and the disappearance of the acetates vibrational modes (data not reported for brevity). The presence of a signal at low distances, with a phase typical of Pd-low Z elements, together with the very small N_{Pd} value must be therefore interpreted as due to subnanometers Pd^0 particles (or "molecular" clusters) significantly interacting with the light elements of the matrix, as almost all Pd atoms are on the surface. This interpretation is perfectly in agreement with FT-IR results, which clearly demonstrated the presence of Py ligands in close proximity of the Pd surface.

On these bases, the fit of the EXAFS data has been extended in the lower R range in order to account for both contributions. On the basis of the chemical affinity,

(95) Frenkel, A. I.; Hills, C. W.; Nuzzo, R. G. *J. Phys. Chem. B* **2001**, *105*, 12689.
(96) Witkowska, A.; Di Cicco, A.; Principi, E. *Phys. Rev. B* **2007**, 76.
(97) Frenkel, A. I. *J. Synchrot. Radiat.* **1999**, *6*, 293.
(98) Bertani, V.; Cavallotti, C.; Masi, M.; Carra, S. *J. Phys. Chem. A* **2000**, *104*, 11390.
(99) Zhang, W. Q.; Ge, Q. F.; Wang, L. C. *J. Chem. Phys.* **2003**, *118*, 5793.

the low-Z element chosen to fit the low R contribution was the nitrogen of the pyridil rings, which is a well-known stabilizing heteroatom for noble metal nanoparticles. The results of the more complete fit are reported in the last column of Table 3 (and Figure S2 in the Supporting Information). About one nitrogen per one Pd atom, at an average distance of 2.011 ± 0.009 Å, is responsible for the low R contribution. Coming to the Pd−Pd contribution, the results confirm those obtained in the fit performed on the Pd−Pd shell only (with an increased significance): $N_{Pd} = 3.9 \pm 0.6$, at $R_{Pd-Pd} = 2.713 \pm 0.007$ Å with a $\sigma^2_{Pd-Pd} = 0.012 \pm 0.001$ Å^{-2}. In case of such small particles, an attempt to correlate coordination number with average particle size is not straightforward because the definition of spherical or cube-octahedral geometries looses its meaning. Similar extremely small N_{Pd} values were already reported by the Kobayashi's group in the case of subnanometer Pd clusters stabilized within micelles of random copolymers.[23] In this case, authors estimated a particle size diameter of 7 Å, by extrapolating the spherical model. More important, a small peak at lower distances was observed also in that case, and assigned to carbon atoms of polymers coordinated with Pd atoms. Even smaller clusters were obtained previously inside zeolites cavities.[94,100−104] In these cases, authors estimated a N_{Pd} value around 5, corresponding to a Pd_{13} stoichiometry. These small clusters were again characterized by a chemical interaction with the support, as revealed by a N_{Pd-O} coordination number around 1.[100,104]

As a final but important observation, EXAFS data analysis on Pd/P4VP reveals that the R_{Pd-Pd} distance shows a significant contraction (0.03 Å) from the bulk value; this is expected for small clusters, where such contractions are described qualitatively in terms of increase of surface stress due to the high curvature of the particles.[105,106] Note that a parallel analysis including the third and fourth cumulants for the Pd−Pd shell was also conducted, in order to verify that the observed contraction of the R_{Pd-Pd} bond distance has a physical meaning.[107] However, in both Pd/PS and Pd/P4VP cases, the new analysis gives (within the experimental error) the same values for all the parameters optimized in the standard analysis, with both third and fourth cumulants being zero within the experimental error.

3.3.4. TEM, FT-IR, and EXAFS: Still Open Controversies. In both Pd/PS and Pd/P4VP samples, the average particle size obtained by TEM is greater than that estimated by EXAFS measurements. The systematic overestimation of the average particle size reflects the well-known difficulty of standard TEM to detect small particles,[41] whereas all metal atoms contribute to the EXAFS signal regardless of the size of the cluster. Moreover, as discussed above, the extraction of quantitative information from EXAFS data requires the definition of an appropriate geometrical model, which is not straightforward in case of very small NPs.[95,97,108,109] It is also possible to assume that electron-beam-induced structural changes and/or sintering of Pd NPs can occur during TEM experiment, as already demonstrated in the literature. Nevertheless, in both Pd/PS and Pd/P4VP cases the discrepancy between EXAFS and TEM results is not negligible and cannot be explained only in these terms. Because the two techniques have been applied exactly on the same samples, we also have to exclude some errors during the activation procedure. Two main explanations, not mutually exclusive, can be provided.

(i) The Pd NPs observed by TEM do really correspond to the totality of Pd particles, but they are not well structurally ordered. It is known that opposite to Pt, Pd particles often result into a well-ordered core surrounded by a disordered external shell. In other words, only one phase is present, but it is characterized by a bimodal distribution of Pd−Pd distances: only the structurally ordered core contributes to the Pd−Pd signal in the EXAFS spectrum, whereas the Pd−Pd contributions of the disordered shell cancel out together. This hypothesis would explain the extremely low intensity of the Pd−Pd contribution in the EXAFS signal, and is in agreement with FT-IR spectra of adsorbed CO, which are typical of NPs and do not show the well-defined components peculiar of molecular Pd carbonyl species.[94] However, it does not fully explain the appearance of the quite significant Pd−N contribution at low R-values in the EXAFS signal of Pd/P4VP. (ii) Together with these NPs, a second Pd phase is present, characterized by clusters having an atomic/molecular dimension (constituted by few atoms), not visible by TEM but well-detected by EXAFS. This possibility is not unrealistic, especially if one considers that the $Pd(OAc)_2$ precursor has a trimeric structure, which can be stabilized by the polymeric support without further aggregation during the reduction step. The fraction of "molecular" clusters should be responsible of the low-R signal observed in the EXAFS spectrum of Pd/P4VP and assigned to Pd−N contribution. Nevertheless, it should be expected that clusters having a "molecular" character give a peculiar IR spectrum of adsorbed CO,[94] which is not observed, unless it is assumed that these clusters are completely shielded by Py ligands.

For the time being, we are not able to definitely confirm neither exclude one of these possibilities. It is clear that we are at the border of reliability for both EXAFS and TEM techniques, because of the lack of a structural model in the first case, and because of the limit in sensitivity in the second case. A more detailed investigation in this

(100) Moller, K.; Bein, T. *J. Phys. Chem.* **1990**, *94*, 845.
(101) Feeley, J. S.; Sachtler, W. M. H. *J. Catal.* **1991**, *131*, 573.
(102) Zhang, Z. C.; Sachtler, W. M. H. *J. Mol. Catal. A* **1991**, *67*, 349.
(103) Zhang, Z. C.; Chen, H. Y.; Sachtler, W. M. H. *J. Chem. Soc., Faraday Trans.* **1991**, *87*, 1413.
(104) Zhang, Z. C.; Chen, H. Y.; Sheu, L. L.; Sachtler, W. M. H. *J. Catal.* **1991**, *127*, 213.
(105) Boswell, F. W. C. *Proc. Phys. Soc.* **1951**, 465.
(106) Lamber, R.; Wetjen, S.; Jaeger, N. I. *Phys. Rev. B* **1995**, *51*, 10968.
(107) Bus, E.; Miller, J. T.; Kropf, A. J.; Prins, R.; van Bokhoven, J. A. *Phys. Chem. Chem. Phys.* **2006**, *8*, 3248.
(108) Boscherini, F.; de Panfilis, S.; Weissmuller, J. *Phys. Rev. B* **1998**, *57*, 3365.
(109) Stern, E. A.; Siegel, R. W.; Newville, M.; Sanders, P. G.; Haskel, D. *Phys. Rev. Lett.* **1995**, *75*, 3874.

direction is behind the scope of the work and would be the topic of a further investigation. The important observation that should be made here is that the polymeric matrix definitely influences the final particle size of Pd NPs; in particular, the pyridil ligands stabilize smaller NPs and act as real surface ligands, as clearly detected by all the techniques employed in this work.

4. Conclusion

Highly cross-linked polymers characterized by a permanent porosity efficiently stabilize very small Pd nanoparticles and affect their final properties. In this work two different DVB-cross-linked polymers have been employed as supports, a poly(ethylstyrene) and a poly(4-vinylpyridine); Pd nanoparticles have been obtained by in situ hydrogen reduction of $Pd(OAc)_2$ precursor. Several spectroscopic techniques (UV−vis, FT-IR, and XAS), coupled with TEM microscopy, have been applied to fully characterize the properties of the obtained Pd/polymer composites in all the synthetic steps, in terms of structural and optical properties, as well as of type and fraction of available surface sites.

It is clearly demonstrated that the formation of Pd nanoparticles and their final properties depend on the nature of the hosting polymers. In particular, the nitrogen-based ligands characterizing the poly(4-vinylpyridine) polymer stabilize smaller nanoparticles with respect to what occurs in the poly(ethylstyrene). In this case, the Pd surface sites experience the proximity of the pyridil ligands (as revealed by EXAFS), with the attendant influence of their electronic properties (as revealed by FT-IR of adsorbed CO and UV−vis spectroscopies). It is expected that the two Pd/polymer systems would show a different behavior in presence of reactants, with promising applications in catalysis.

Acknowledgment. Riccardo Pellegrini, Giuseppe Leofanti and Anatoly Frenkel, are kindly acknowledged for the useful discussion. Sergej Nikitenko and all the staff of BM26A beamline at ESRF (Grenoble) are acknowledged for the helpful support during the XAS measurements (proposal CH-2766).

Supporting Information Available: Additional figures (PDF). This material is available free of charge via the Internet at http://pubs.acs.org.